

# Use of UHPC slab for continuous composite steel-concrete girders

Alfarabi M. Sharif<sup>a</sup>, Nizar A. Assi<sup>b</sup> and Mohammed A. Al-Osta<sup>\*</sup>

Department of Civil Engineering, King Fahd University of Petroleum & Minerals, Dhahran 31261, Saudi Arabia

(Received December 5, 2018, Revised December 28, 2019, Accepted December 29, 2019)

**Abstract.** The loss of composite action at the hogging moment zone for a continuous composite girder reduces the girder stiffness and strength. This paper presents an experimental investigation of the use of an ultra-high performance concrete (UHPC) slab at the hogging moment zone and a normal concrete (NC) slab at the sagging moment zone. The testing was conducted to verify the level of loading at which composite action is maintained at the hogging moment zone. Four two-span continuous composite girders were tested. The thickness of the UHPC varied between a half and a full depth of slab. The degree of shear connection at the hogging moment zone varied between full and partial. The experimental results confirmed the effectiveness of the UHPC slab to enhance the girder stiffness and maintain the composite action at the hogging moment zone at a load level much higher than the upper service load limit. To a lesser degree enhanced performance was also noted for the smaller thickness of the UHPC slab and partial shear connection at the hogging moment zone. Plastic analysis was conducted to evaluate the ultimate capacity of the girder which yielded a conservative estimation. Finite element (FE) modeling evaluated the girder performance numerically and yielded satisfactory results. The results indicated that composite action at the hogging moment zone is maintained for the degree of shear connection taken as 50% of the full composite action and use of UHPC as half depth of slab thickness.

**Keywords:** ultra-high performance concrete; composite action; continuous composite girders; finite element model; plastic analysis

## 1. Introduction

Composite construction has been extensively used in bridges and buildings in recent years. Composite steel-concrete construction is used by combining these two construction materials (Xiang *et al.* 2015, Zhou M. *et al.* 2016, Wang *et al.* 2017). Composite steel-concrete construction provides an efficient and cost-effective form of construction due to a reduction in member depth, savings in steel weight, and the rapid construction process. The composite action between the concrete slab and the steel beam is formed by providing the shear connectors. The shear connectors contribute to the shear transfer and prevent uplift (Kim *et al.* 2011, Vasdravellis and Uy 2014, Thirumalaiselvi *et al.* 2016). Composite action is characterized by the number of shear studs, and it can be full or partial composite action (Rodrigues and Laím 2014, Zhan *et al.* 2016). Therefore, degree of shear connection between concrete slab and steel beam was investigated in literature to study the effects of the shear connection on the performance of composite girders (Kim *et al.* 2015, Ding *et al.* 2016, Fang *et al.* 2016, Liu *et al.* 2016, Zhou W. *et al.*

2016). In composite girders, optimal use of the composite action will be at the sagging moment where the concrete and steel are under compression and tension, respectively. However, the concrete slab at the hogging moment zone of the continuous composite steel-concrete girders is subject to tension and consequently loses its contribution to the composite action.

The American Institute of Steel Construction AISC (2005) code either ignores the contribution of the concrete slab at the hogging moment zone for continuous composite girders or considers the steel reinforcements of the concrete slab to act compositely with the steel section. For both options of the AISC code, the section capacity at the hogging moment zone is greatly reduced.

Researchers have tried different schemes to maintain the composite action at the hogging moment zone for continuous composite girders. (Basu *et al.* 1987a, b) evaluated analytically and experimentally the behavior of a continuous composite steel-concrete beam by prestressing the concrete slab while it is fully composite with the steel beam at the hogging moment zone. The results indicated that cracks in the concrete slab were prohibited at the service load, while the load carrying capacity was increased by 20%. External prestressing applied directly to the steel girder was evaluated experimentally by (Elremaily and Yehia 2006, Chen *et al.* and Jia 2009 and Nie *et al.* 2011). The results showed improvements in the service load, stiffness and strength of the continuous composite girder. Sharif *et al.* (2015) investigated experimentally the use of a carbon fiber-reinforced polymer (CFRP) sheet bonded to

\*Corresponding author, Ph.D.

E-mail: malosta@kfupm.edu.sa

<sup>a</sup>Ph.D. Professor

E-mail: fmsharif@kfupm.edu.sa

<sup>b</sup>Ph.D. Student

E-mail: g201306590@kfupm.edu.sa

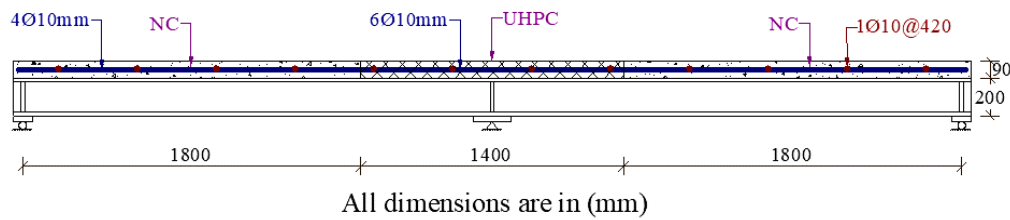


Fig. 1 Detailed dimensions of the composite steel-concrete girder

the top of a concrete slab at the hogging moment zone. The results indicated that the composite action at the hogging moment zone is maintained thus preventing crack initiation in the concrete slab for service loads. Samaaneh *et al.* (2016) conducted a numerical investigation of continuous composite steel-concrete girders strengthened with CFRP by using the ABAQUS software. The results were validated experimentally and it was demonstrated that the thickness of the CFRP sheet depends on the adhesive strength and the capacity of the girder at the sagging moment. (Lin and Yoda 2013, Lin *et al.* 2013) investigated the mechanical properties of simply supported composite steel concrete girders at the hogging moment. Eight inverted simply supported beams were prepared and tested to study the effect of three different variables including the type of loading, steel fiber-reinforced concrete, and a rubber-latex mortar coating on the behavior of the composite girders. The study showed that steel fiber-reinforced concrete controls the initiation of cracks and the width of the cracks.

The contribution of the current research is to evaluate experimentally the use of a UHPC slab at the hogging moment zone and an NC slab at the sagging moment zone for continuous composite girders. The experimental investigation included limited testing to assess the effects of the thickness of the UHPC slab and the degree of shear connection at the hogging moment zone. A theoretical evaluation using plastic analysis determined the girder's ultimate capacity. The girder's behavior was evaluated numerically via finite element modeling using the commercial software ABAQUS. A numerical solution was utilized to properly evaluate the effect of the degree of shear connection and the UHPC slab thickness at the hogging moment zone.

## 2. Experimental program

The dimension details of the two-span continuous composite girders tested in this program is shown Fig. 1. The concrete slab was cast using UHPC at the hogging moment zone located between the inflection points and NC slab at the sagging moment zone as shown in Figs. 2(a) and 2(b), respectively. The hot-rolled steel section was proportioned to eliminate any secondary failure, including local buckling, web yielding, web crippling, and lateral-torsional buckling. The cross-section dimensions for the girders are shown in Fig. 3. Minimum steel reinforcement was provided in the NC slab as per the ACI Code (Committee, Institute and Standardization, 2008). The steel reinforcement in the UHPC slab was provided according to

the AASHTO code (AASHTO, 2007). Shear studs 19-mm in diameter were fillet welded to the top flange of the steel section and embedded to a length of 60-mm in the concrete slab. All four girders were designed to develop full composite action between the NC slab and steel girder at the sagging moment zone. The shear stud spacing for the sagging moment zone is shown Fig. 4. The test variables for the girders are limited to the hogging moment zone considering the degree of shear connection and thickness of UHPC slab as given in Table 1. Girder G1 is the control specimen with NC slab and designed to develop full composite action. Girder G2 with UHPC slab and design to develop full composite action. Girder G3 was designed to develop full composite action and its slab composed of two parts the bottom slab thickness is NC and the top slab thickness is UHPC. Girder G4 with UHPC slab was designed as partially composite.



Fig. 2 Casting of concrete slabs

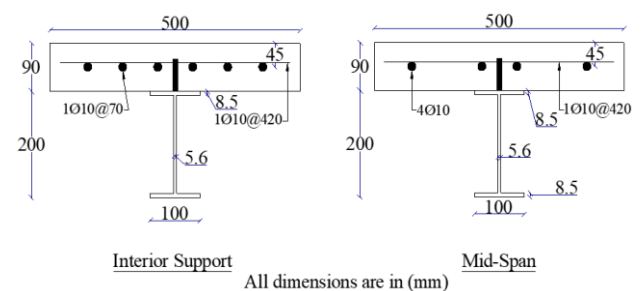


Fig. 3 Composite girder's cross sections

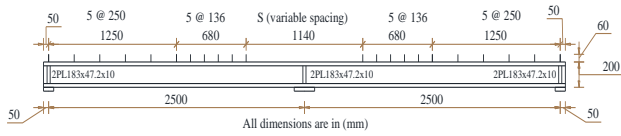


Fig. 4 Detailed dimensions of steel girder and studs spacing

Table 1 Test variable at hogging moment zone

Girder No.	Composite action	Stud Spacing (mm)	Slab Thickness (mm)	
			UHPC	NC
G1	Full	127	0	90
G2	Full	127	90	0
G3	Full	127	45	45
G4	Partial	228	90	0

2.1 Materials

The concrete mix design and mechanical properties for NC and UHPC are given in Tables 2 and 3, respectively. The compressive strength test was conducted according to ASTM C39 specification. The flexural strength test was conducted according to ASTM C293 specification. The compressive and tensile stress-strain for NC and UHPC are shown in Figs. 5(a) and 5(b) and Figs. 6(a) and 6(b), respectively.

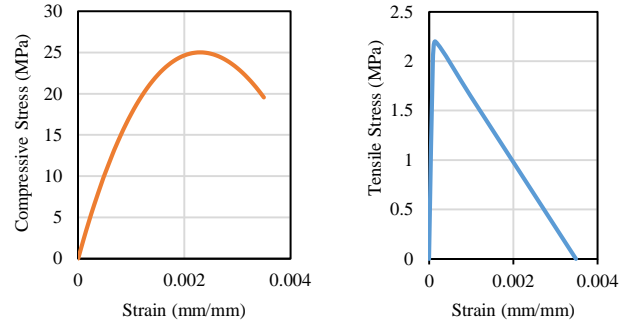
The mechanical properties of the structural steel and steel reinforcement (Table 4) were conducted according to ASTM E8M and ASTM A370 specification, respectively. The stress-strain curves for structural steel and steel are shown in Figs. 7(a) and 7(b), respectively.

Table 2 Concrete mix design

NC		UHPC (Ahmad <i>et al.</i> 2016)	
Mix component	Weight (Kg/m <sup>3</sup> )	Mix component	Weight (Kg/m <sup>3</sup> )
Portland Cement	345	Portland Cement	900
Water	217.3	Water	168
Coarse Aggregate	1074	Fine Sand	980
Fine Aggregate	725.6	Superplasticizer	40.3
		Steel Fibers	157
		Micro-Silica	220

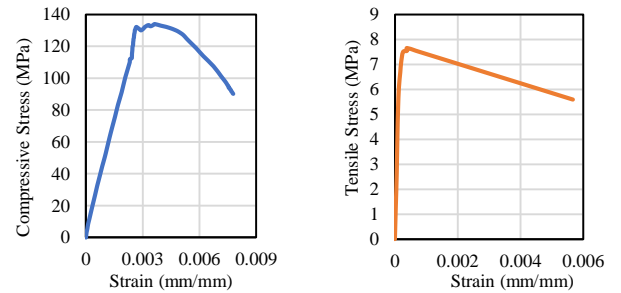
Table 3 Mechanical properties of concrete

Mechanical Property	NC	UHPC
Compressive Strength (MPa)	25	134
Tensile Strength (MPa)	2.2	7.7
Flexural strength (MPa)	4.28	28
Poisson's Ratio ( $\nu$ )	0.17	0.16
Young's Modulus (MPa)	20283	47,000



(a) Compression (b) Tension

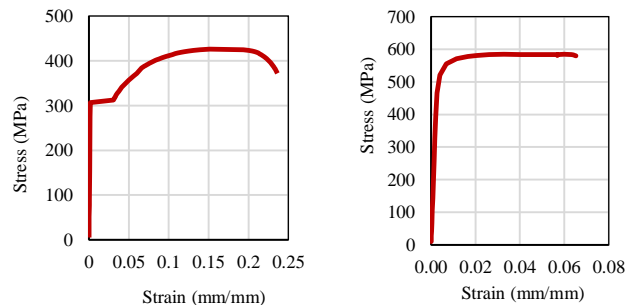
Fig. 5 Stress-strain diagrams for NC



(a) Compression (b) Tension

Fig. 6 Stress-strain diagrams for UHPC

The shear capacity of the studs for NC and UHPC was evaluated by a push-out test according to Eurocode 4 (2004). A steel section with two shear studs on each side was cast with concrete as shown in Fig. 8. A linear variable differential transducer (LVDT) was fixed at the bottom of the steel section to measure the slip corresponding to the load applied at the top of the steel section. The measured load versus the shear connection slip is shown in Fig. 9 for NC and UHPC. The failure of the NC slab was due to the bearing failure in the concrete, while the failure of the UHPC slab was due to shear failure in the welding material of stud, as shown in Fig. 10. In this study, the test was conducted under static loading.



(a) Structural steel (b) Steel Reinforcement

Fig. 7 Tensile stress-strain diagrams

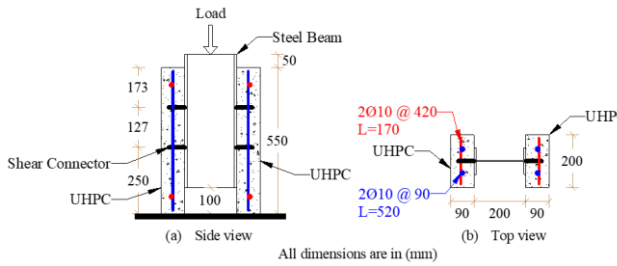


Fig. 8 Schematic diagram for the two-way push-out test

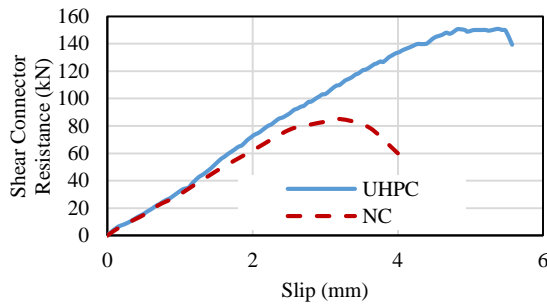


Fig. 9 Load-slip curve



Fig. 10 Shear failure of welding material connecting stud to top flange

Table 4 Mechanical properties of steel

Mechanical Property	Structural	Steel
	Steel	Reinforcement
Yield Strength (MPa)	306	555
Ultimate Strength (MPa)	425	585
Poisson's Ratio ( $\nu$ )	0.27	0.3
Young's Modulus (GPa)	193	171

## 2.2 Test Set-up and Instrumentation

The composite girders were tested under a five-point bending test. A lateral support was provided at the interior support to prevent lateral-torsional buckling of the compression flange. The schematic and experimental test set-up are shown in Figs. 11(a) and 11(b). The composite girders were tested under monotonic loading at a rate of loading of 0.5 kN/s. The load was equally applied at the mid of each span as a concentrated line load at the top of the slab. LVDTs were placed at the mid of each span to measure deflection. Thirty-nine strain gauges were used to measure the strain in the steel and the concrete at the mid-span and over the interior support as shown by Fig. 12. All of the instrumentation was connected to control the data logger to record the load, the strains, and the displacement.

A white wash was applied over the surface of the UHPC/NC slab to help with detecting the development of cracks.

## 2.3 Experimental results and discussion

The effectiveness of using a UHPC slab at the hogging moment zone is demonstrated by the direct comparison of the experimental results for girder G2 with the control girder G1. The stiffness and slight strength improvement for girder G2 is clearly observed in Fig. 13. To assess the slab integrity at the hogging moment zone, the ratio of the cracking load to the yielding load  $\lambda$  is taken as the indication of the level at which the concrete slab maintained its composite action under the service load. The cracking load  $P_{cr}$  is defined as the load-initiating of the visible cracks over the interior support. The yielding load  $P_y$  is taken as the upper limit of the service load at which yielding of the girder's bottom flange at the sagging moment zone occurs. The values of the  $P_{cr}$  and  $P_y$ , recorded from test observations, are shown in Table 5. Girder G2 exhibited considerably higher values of  $P_{cr}$  and  $\lambda$  than girder G1. This clearly confirms the effectiveness of the UHPC slab in maintaining the composite action at the hogging moment zone at a load much higher than the upper service load limit.

The use of the combined UHPC top layer and the NC bottom layer of the slab at the hogging moment zone is demonstrated by girder G3. Considerable improvements in terms of the  $P_{cr}$  and the  $\lambda$  for girder G3 relative to girder G1 but not, as expected, equivalent to that of girder G2. The cracking load of girder G3 was associated with the delamination between the upper UHPC and the bottom NC layer of the slab as shown in Fig. 14. This premature failure limited the full utilization of the UHPC slab to maintain the composite action for the higher load.

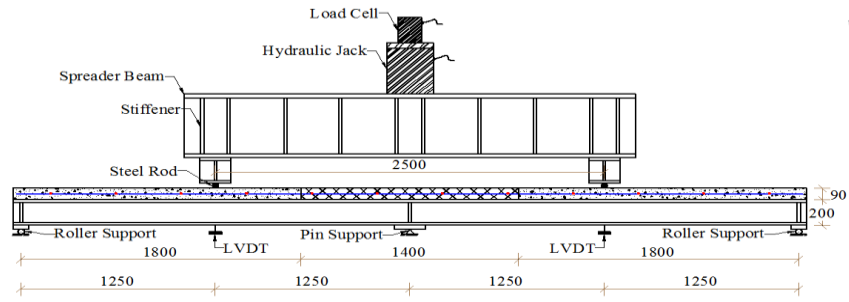
The degree of shear connection at the hogging moment zone for girder G4 is reduced by 50% relative to girder G2. The relative slip between the UHPC slab and the steel section for girder G4 and girder G2 are evident from the measured strains at a 50 kN load, as shown in Fig. 15. The partial connection level for girder G4 reduced its stiffness, the cracking load and the  $\lambda$  values relative to girder G2 by 20%, 13% and 11%, respectively.

### 2.3.1 Ultimate Moment Capacity

Based on the measured strain, the moment capacities of the girders at positive moment locations ( $M_{+ve}^*$ ) and negative moment locations ( $M_{-ve}^*$ ) were calculated and listed in Table 6.

Table 5 Experimental values for cracking, yielding and ultimate loads

Girder	$P_{cr}$ (kN)	$P_y$ (kN)	$\lambda$	Ultimate load ( $P_u$ ) (kN)
G1	57	171	0.33	242
G2	247	188	1.31	262
G3	186	175	1.06	250
G4	215	179	1.20	247



All dimensions are in (mm)

(a) Schematic diagram



(b) Experimental test

Fig. 11 Test set-up of composite girders

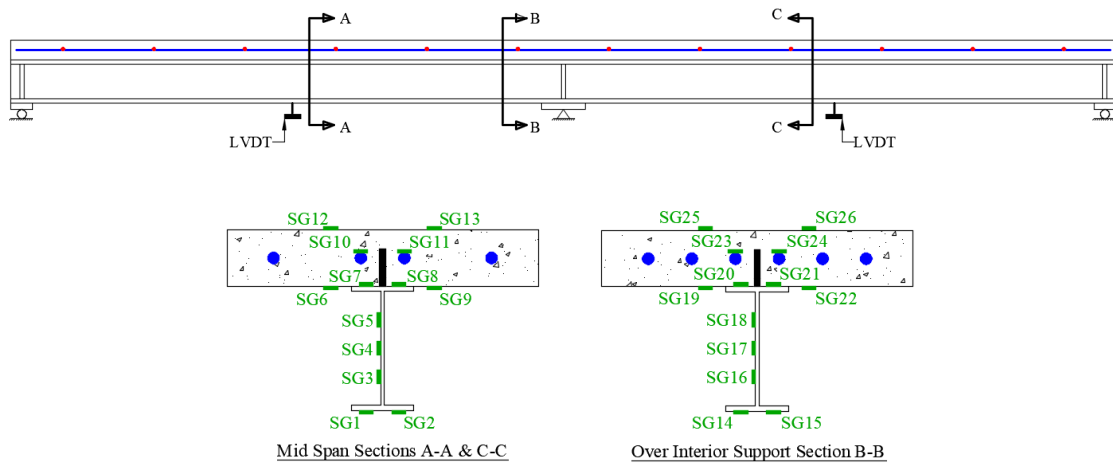


Fig. 12 Locations and distributions of strain gauges

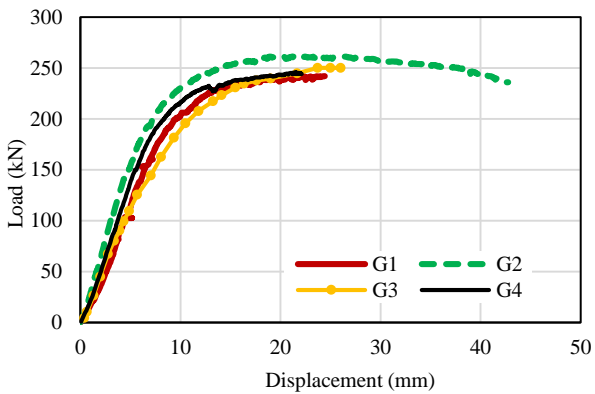


Fig. 13 Experimental load-displacement curves



Fig. 14 Developed cracks in concrete slab over the interior support at ultimate load

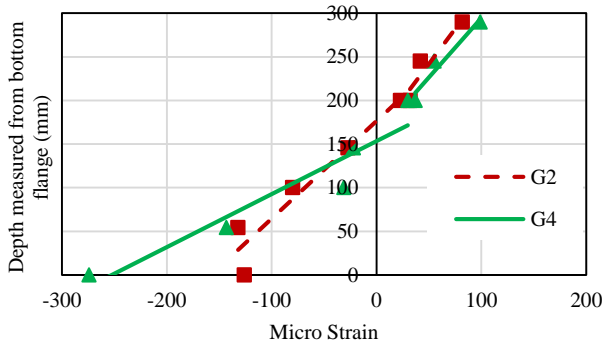


Fig. 15 Experimental strain distribution at interior support section at service load

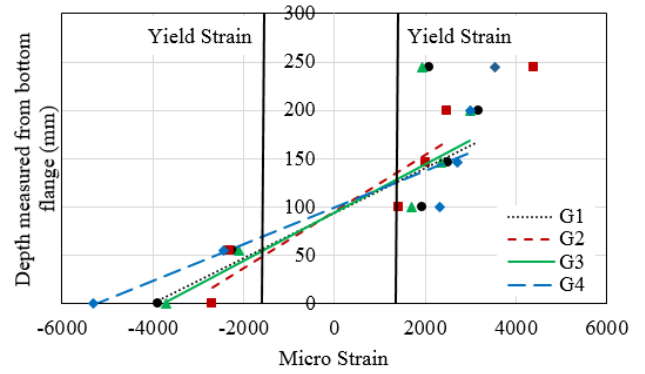


Fig. 18 Experimental strain distribution at interior support section at ultimate load



Fig. 16 Shear-compression failure at mid-span

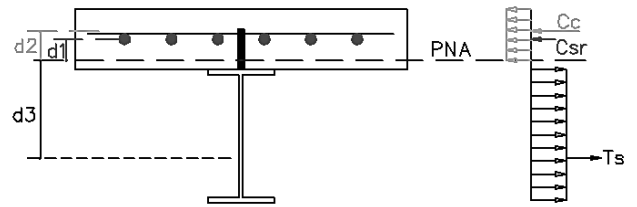


Fig. 19 Stress distribution at sagging moment section at ultimate condition

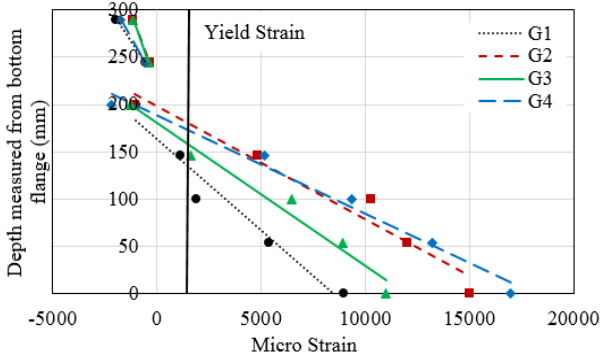


Fig. 17 Experimental strain distribution at mid-span section at ultimate load

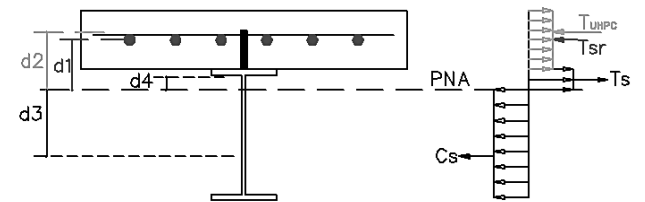


Fig. 20 Stress distribution at hogging moment section at ultimate condition

Theoretical values for the girder's ultimate positive and negative moment capacities were evaluated as follows, assuming the stress distributions shown in Figs. 19 and 20, which corresponded to the elastic-plastic behavior of the steel without strain hardening

$$\bar{M}_{+ve} = C_{sr} \times d_1 + C_{cc} \times d_2 + T_s \times d_3 \quad (1)$$

$$\bar{M}_{-ve} = T_{sr} \times d_1 + C_s \times d_3 + T_s \times d_4 \quad (2)$$

$$\bar{M}_{-ve} = T_{sr} \times d_1 + T_{UHPC} \times d_2 + C_s \times d_3 + T_s \times d_4 \quad (3)$$

Eq. (2) is used to evaluate the ultimate moment capacity with no UHPC at the hogging moment zone. While Eq. (3) includes the contribution of the UHPC slab to the hogging moment capacity. In Eqs. (1)-(3),  $C_{sr}$ ,  $C_{cc}$ , &  $C_s$  are the compression forces in the reinforcements, the NC slab and the steel section, respectively.  $T_{sr}$ ,  $T_s$ , &  $T_{UHPC}$  are the tension forces in the steel reinforcement, steel section and the UHPC slab, respectively. Theoretical values for  $\bar{M}_{+ve}$  and  $\bar{M}_{-ve}$  are shown in Table 6.

### 2.3.2 Plastic analysis

Plastic analysis is used to predict the flexural failure load for continuous composite girders. The theoretical value of the load ( $P_f$ ) necessary to cause failure in the composite girders is given as

$$P_f = \left[ \frac{2(2\alpha + 1)}{L} \right] M_{-ve} \quad (4)$$

where  $L$  is the span length;  $M_{ve}$  is the hogging moment capacity; and  $\alpha$  is the ratio between the sagging and the hogging moment capacity.

The analytical failure loads ( $\bar{P}_f$ ) calculated assuming elastic-perfect plastic material behavior and the evaluated failure loads ( $P_f^*$ ) based on the experimental strain measurements are summarized in Table 6. The obtained failure load  $\bar{P}_f$  is lower than  $P_f^*$  as expected since the strain hardening of the materials is ignored. Table 6 demonstrates that the predicted ultimate loads ( $\bar{P}_f, P_f^*$ ) calculated by Eq. (4) are lower than the ultimate load ( $P_u$ ) obtained from the experimental testing. Plastic analysis underestimates the failure load and leads to safe load expectations.

### 3. Numerical investigation

A 3D Finite Element (FE) modeling of the continuous composite girders with NC and UHPC slabs at the hogging moment zone was developed utilizing the ABAQUS software. In this study, a dynamic explicit approach was used to overcome the convergence problems accompanied by softening of the concrete slab under tension. The developed model includes material and geometrical nonlinearities and different interface contact methods between the different materials to simulate the actual behavior of the composite girders.

#### 3.1 Finite element modeling

##### 3.1.1 Geometry model

The geometry of the composite girder consisting of NC slab, UHPC slab, structural steel, transverse stiffeners, bearing plates (over supports under the applied loads) and the shear studs, is shown in Fig. 21.

##### 3.1.2 Finite element types

A C3D8R 8-noded linear brick, reduced integration, and hourglass control element was utilized to model NC slab, UHPC slab, structural steel, transverse stiffeners, a rigid bearing plates and shear studs. A two-node linear 3-D truss (T3D2) element was used to model the longitudinal and transverse slab reinforcements.

##### 3.1.3 Mesh size sensitivity

Mesh-sensitivity analysis was conducted to check the optimum mesh size of the element that should be used for the model. Four mesh sizes were checked ranging from 25 to 65 mm to investigate mesh size sensitivity. The results of numerical load-displacement curves for the model with different mesh sizes are shown in Fig. 22. Based on the accuracy and rational running time, the mesh size of 45 mm was considered as shown in Fig. 23.

##### 3.1.4 FE Interaction Modeling

The interaction between the different components was modeled using different types of contact properties.

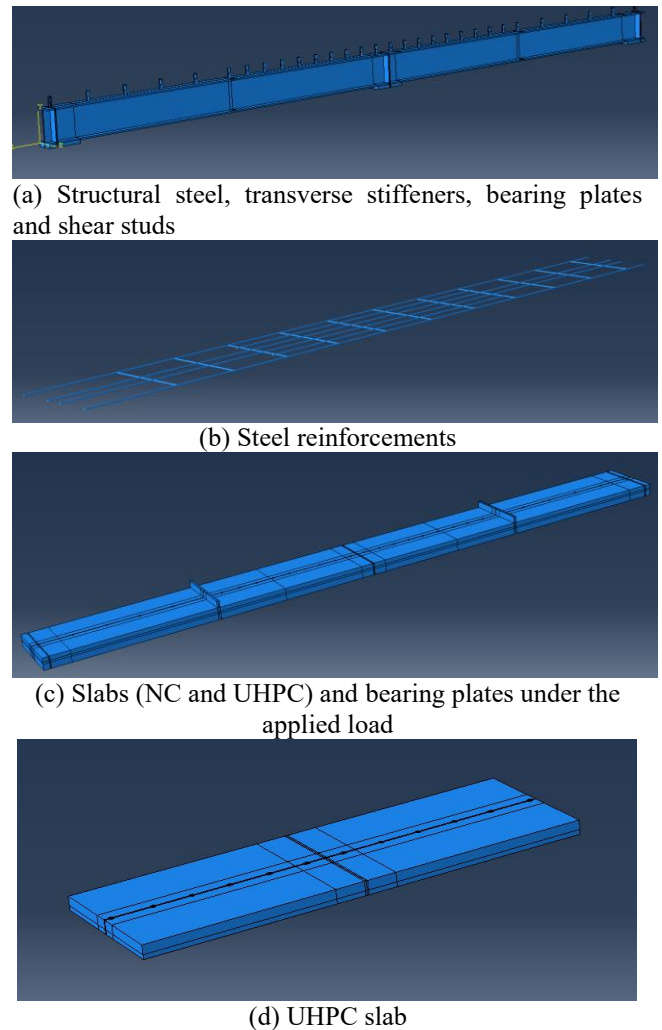


Fig. 21 Geometry of composite girder

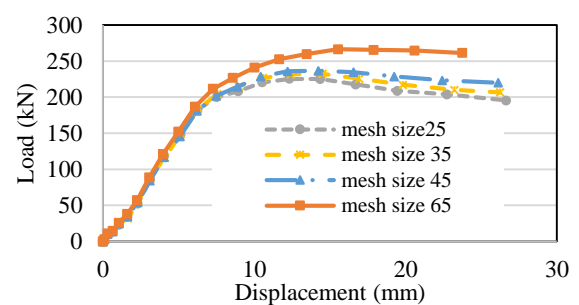


Fig. 22 Effect of mesh size (mm) on load-deflection curves

The interaction between the shear connectors and the structural steel was represented using a tie interaction (perfect bond). Similarly, tie interaction was applied between the stiffeners and the structural steel. The interaction between the steel reinforcements and the concrete slab was defined using an embedded technique in ABAQUS (Simulia 2013) in which the reinforcements were modeled as embedded elements, while the concrete slab was considered as the host region.

Table 6 Experimental and analytical moment capacities and corresponding failure loads

Girder	$P_u$ (kN)	$M_{+ve}^*$ (kN.m)	$M_{-ve}^*$ (kN.m)	$\alpha$	$P_f^*$ (kN)	$P_f^*/P_u$	$\bar{M}_{+ve}$ (kN.m)	$\bar{M}_{-ve}$ (kN.m)	$\alpha$	$\bar{P}_f$ (kN)	$\bar{P}_f/P_u$
G1	242	111.8	71.8	1.557	236.3	98%	109.01	71.63	1.522	231.7	96%
G2	262	117.9	89.2	1.322	260	99%	109.01	96.02	1.135	251.2	96%
G3	250	112.5	78.6	1.431	242.9	97%	109.01	76.72	1.421	235.8	94%
G4	247	110.5	84.6	1.306	244.5	99%	109.01	75.8	1.438	235.1	95%

Table 7 Input parameters of CDP model

	Young's Modulus (MPa)	Poisson's Ratio	Dilatation Angle (degree)	Eccentricity	$f_{bo}/f_{co}$	K	Viscosity parameter
NC	20283	0.199	36	0.1	1.16	0.67	0
UHPC	47000	0.16					

The interaction modeling between the shear studs and the concrete slab was specified as a hard contact in the normal direction and friction interaction with a 0.2-coefficient of friction in the tangential direction. The hard contact was used in the normal direction to avoid penetration of the shear connectors into the concrete slab. In the same way, the hard contact in the normal direction and friction interaction with a 0.4-coefficient of friction in the tangential direction were utilized to represent the interaction between the NC and the UHPC layers.

### 3.1.5 Boundary Conditions and load Application

The end supports are modeled as roller supports in which they are restrained in the vertical and transverse directions ( $U_y = 0$  and  $U_x = 0$ ). The intermediate support is modeled as pin supports in which it is restrained in the vertical, horizontal and transverse directions ( $U_y = 0$ ,  $U_x = 0$  and  $U_z = 0$ ). The concentrated loads have been applied at the mid-span using steel plates to transfer the load uniformly (Fig. 24).

### 3.1.6 Modeling of NC and UHPC

The behavior of quasi-brittle NC and UHPC can be simulated by many conceptual models available in literature, which include a discrete crack model, smeared crack model and concrete damage plasticity model (CDP). In this study, the CDP model as developed by Lubliner *et al.* (1989) and extended by Lee and Fenves (1998) was utilized to simulate the behavior of concrete under both tension and compression. ABAQUS was used to model the behavior of composite girders based on the mechanical properties obtained from the experimental work. The input parameters of the CDP model are those shown in Table 7 and the stress-strain diagrams for NC and UHPC are shown in Figs. 5(a) and 5(b) and Figs. 6 (a) and 6(b), respectively.

Concrete damage parameters  $d_c$  and  $d_t$  used to simulate the cracking under compression and tension, respectively were proposed by Birtel and Mark (2006) and given by Eqs. (5) and (6).

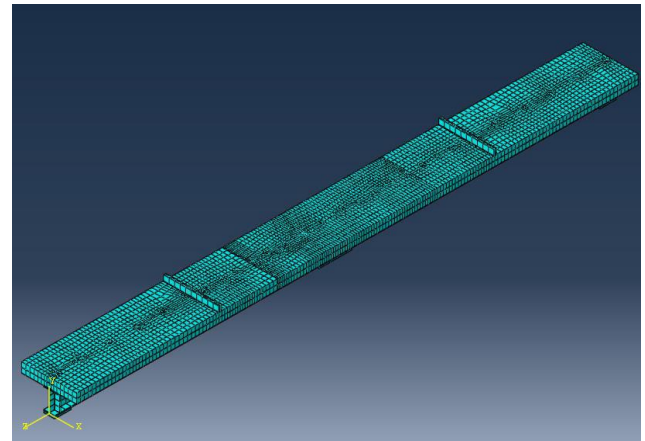


Fig. 23 Meshing of the composite girder

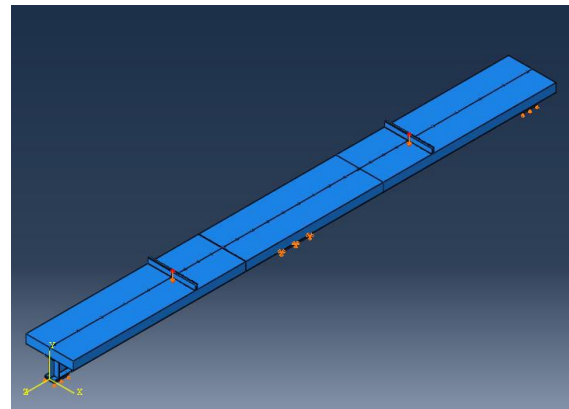


Fig. 24 Boundary conditions and applied load

$$d_c = 1 - \frac{f_c E_c^{-1}}{\varepsilon_c^{pl} \left( \frac{1}{b_c} - 1 \right) + f_c E_c^{-1}} \quad (5)$$

where:

- $d_c$  = Concrete compression damage parameter
- $f_c$  = Compressive stress
- $E_c$  = Modulus of elasticity of concrete
- $\epsilon_c^{pl}$  = Plastic strain corresponding to compressive strength
- $b_c$  = Constant ranges  $0 < b_c < 1$

$$d_t = 1 - \frac{f_t E_c^{-1}}{\epsilon_t^{pl} \left(\frac{1}{b_t} - 1\right) + f_t E_c^{-1}} \quad (6)$$

where:

- $d_t$  = Concrete tension damage parameter
- $f_t$  = Tensile stress
- $E_c$  = Modulus of elasticity of concrete
- $\epsilon_t^{pl}$  = Plastic strain corresponding to Tensile strength
- $b_t$  = Constant ranges  $0 < b_t < 1$

### 3.1.7 Modeling of structural steel and rebar

Structural steel and reinforcements steel were modeled as an elastic-plastic material including strain hardening. The elastic behavior of the materials was represented by Young’s modulus ( $E$ ) and Poisson’s ratio ( $\nu$ ), while the stress-strain curve was used to model the nonlinear plastic behavior. Table 4 shows the mechanical properties of different materials of steel. Figs. 7(a) and 7(b) show the stress versus strain relationship for structural steel and reinforcements steel, respectively.

### 3.2 Finite element validation

The developed models were validated using the results of the experimental tests of the four girders in which the load vs. deflection curves, cracking, yielding and ultimate load and damage patterns from the experimental and FE model works were compared. The comparison of load-displacement curves for the four girders is shown in Fig. 25. The FE modeling showed a greater stiffness of girders as compared to the experiment. However, it can be observed that the total response of all girders is in good agreement with the experiment results. The FE model predicted the ultimate load capacities of the girders G1, G2, G3, and G4 are 237 kN, 256 kN, 243 kN, and 244 kN, which are 2%, 2%, 3%, and 1% higher than the conforming test values, respectively. In addition, it was found that the difference between the FE cracking and yielding loads of the specimens and the experiment values is less than 4% and 1%, respectively, (Table 8). Additionally, the FE model predicted the failure modes similar to those observed in experimental results (Fig. 26). It can be seen that the developed model is capable of detecting UHPC failure mode at the hogging moment zone and the shear-compression failure mode at the mid-span region.

### 3.3 Parametric study

With the limited experimental results on the effect of the degree of shear connection and the UHPC thickness at hogging moment zone on the performance of composite girders, the verified model was employed to assess these two variables.

### 3.3.1 Shear connection

The effect of the shear connection at the hogging moment zone on the behavior of continuous composite girders was investigated considering six different stud spacings, as shown in Table 9.

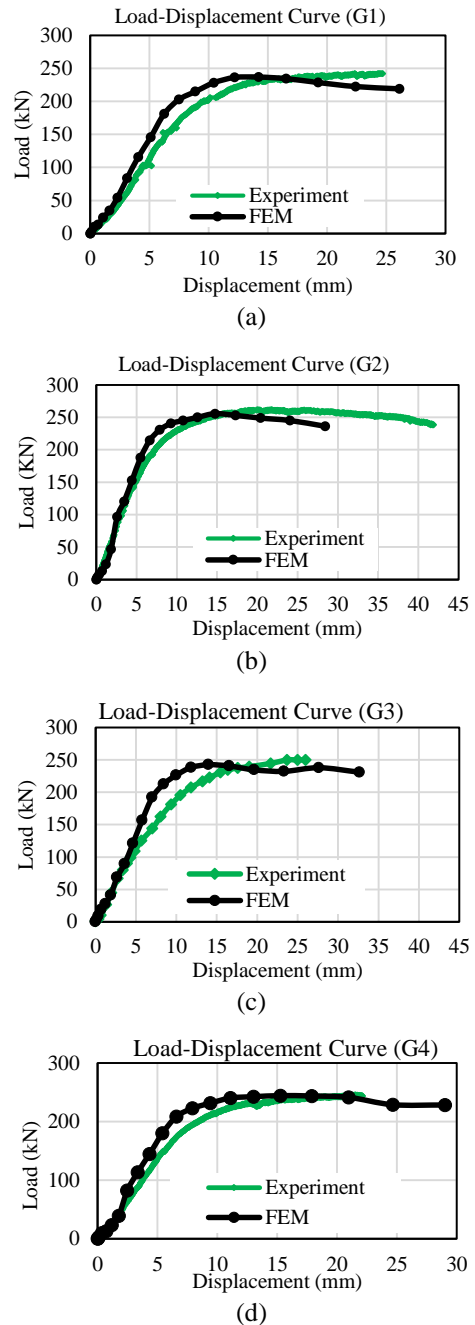
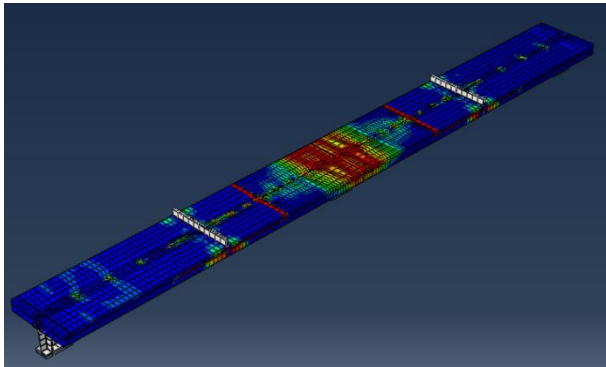


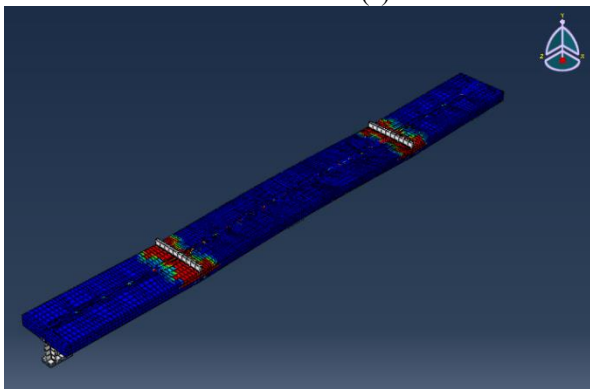
Fig. 25 Comparison of numerical and experimental load deflection curves

Table 8 Experimental and analytical values for cracking, yielding and ultimate loads

Girder	Cracking load (kN)			Yielding load (kN)			Ultimate load (kN)		
	Exp.	FE	% Difference	Exp.	FE	% Difference	Exp.	FE	% Difference
G1	57	55	4%	171	169	1%	242	237	2%
G2	247	243	2%	188	187	1%	262	256	2%
G3	186	181	3%	175	173	1%	250	243	3%
G4	215	208	3%	179	178	1%	247	244	1%



(a) Detected UHPC cracks at hogging moment zone



(b) Shear-compression failure mode at mid-span



Fig. 26 Girder at failure stage

Besides the experimentally tested girders (G2 and G4), an additional four girders (G2-1, G2-2, G2-3 and G2-4) were modeled in the ABAQUS software.

Girder G2 has a full degree of shear connection at the hogging zone. Girder G2-1 is considered to have a higher degree of shear connection than girder G2. Girders (G2-1, G2-2 and G2-3) are with partial shear connection levels. Shear stud spacing slightly affected the ultimate capacity and stiffness of the composite girders as illustrated in Fig. 27.

The interface slip between the top of the steel flange and the bottom of the UHPC slab versus loading for all girders are shown in Fig. 28 and summarized in Table 9. It is obvious that the slip decreases with a higher degree of shear connection. The cracking load, yielding load and  $\lambda$  for all girders are given in Table 9. The values for  $\lambda$  decrease with a lower degree of shear connection. Girder G2-3 indicates that  $\lambda$  is close to one, which represents a satisfactory shear connection level to maintain the composite action at the

hogging moment zone. Therefore, it can be concluded that the degree of shear connection at hogging moment zone can be taken as 50% of the full composite action.

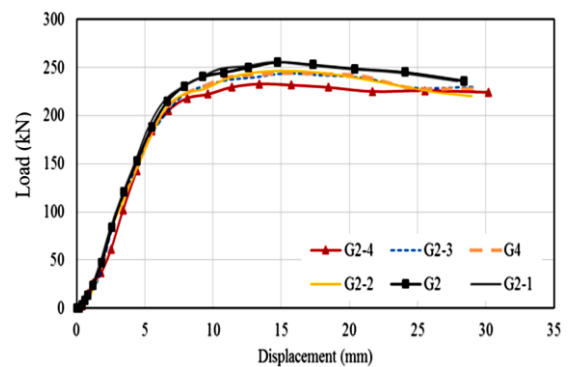


Fig. 27 Load-deflection curves for varying shear connection levels at hogging moment zone

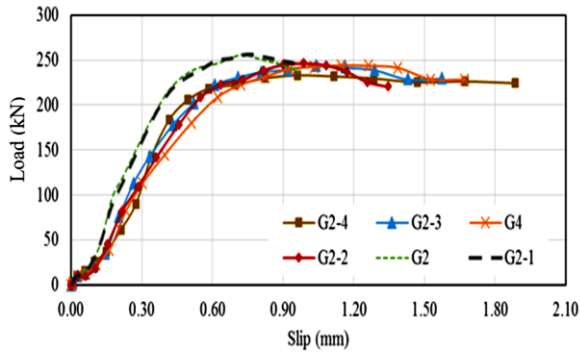


Fig. 28 Load-slip curves for varying shear connection levels at hogging moment zone

Table 9 Interface slip, cracking and yielding loads corresponding to the different shear connections

Girder	Number of Stud @ Spacing mm	Interface Slip (mm)	$P_{cr}$ (kN)	$P_y$ (kN)	$\lambda = P_{cr}/P_y$
G2-1	12@103.6	0.97	243	187	1.30
G2	10@127	0.97	243	187	1.30
G2-2	8@163	1.35	227	184	1.23
G4	6@228	1.67	208	178	1.17
G2-3	4@380	1.73	179	173	1.03
G2-4	2@1140	1.88	154	171	0.90

### 3.3.2 UHPC Thickness

The study assumed two concrete layers at the hogging moment zone. The top layer is UHPC and the bottom one is NC. Besides the experimentally tested girders (G1, G2 and G3), an additional two girders (G1-1 and G1-2) were considered to investigate the effects of the UHPC thicknesses at the hogging moment zone.

The performance of girder G1-1 with a UHPC slab thickness equivalent to one quarter slab depth has not shown any improvement relative to the control girder G1 as shown in Fig. 29 and Table 10.

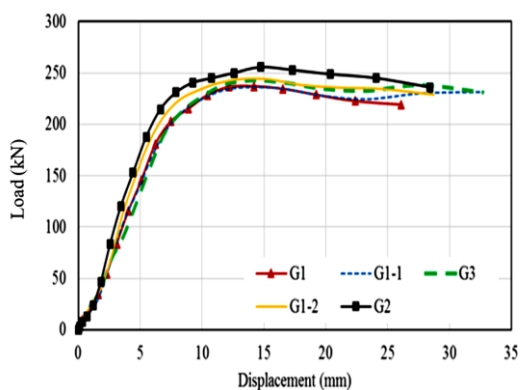


Fig. 29 Load-deflection curves for varying UHPC thickness

Table 10 Cracking, yielding and ultimate loads corresponding to UHPC thickness

Girder	UHPC Slab Thickness (mm)	$P_{cr}$ (kN)	$P_y$ (kN)	$\lambda$	$P_u$ (kN)
G1	0 (90-mm NC)	55	169	0.33	237
G1-1	22.5	55	169	0.33	236.1
G3	45	181	173	1.05	242.9
G1-2	67.5	219	181	1.21	244.3
G2	90	243	187	1.30	255.7

This is mainly attributed to the fact that shear studs do not penetrate the UHPC slab thickness. It is clearly from Fig. 29 and Table 10 that as the UHPC slab thickness increases for girders (G3, G1-2 and G2), their performance improved in terms of the stiffness and  $\lambda$  values. Girder G3 with a UHPC slab thickness of half the depth of the slab gives a  $\lambda$  value close to one which represents a satisfactory UHPC slab thickness necessary to maintain the composite action at the hogging moment zone. Therefore, it can be concluded that using half UHPC slab thickness at hogging moment zone is sufficient to achieve the desired performance.

## 4. Conclusions

Based on the experimental and numerical evaluations for the use of UHPC slab at hogging moment zone, the following can be concluded:

- The use of a UHPC slab at the hogging moment zone maintained the composite action at a load level much higher than the upper service load limit and greatly improved the stiffness;
- The predicted failure load using plastic analysis is a reasonable and safe estimate compared to the experimental failure load;
- The degree of shear connection can be taken as 50 % of full composite action at negative moment region to achieve the required performance of the continuous composite girder; and
- The use of half UHPC slab thickness at hogging moment zone is sufficient to achieve the desired performance of the continuous girder.

## Acknowledgments

Financial support for this work, provided by King Fahd University of Petroleum and Minerals, Civil and Environmental Department and the Deanship of Scientific Research under project number **IN171047**, is gratefully acknowledged.

## References

- AASHTO, L. (2007), "AASHTO LRFD bridge design specifications", Transportation (Amst); American Association of State Highway and Transportation Officials, Inc.: Washington, DC.
- AISC, C. (2005), "Steel construction manual", American Institute of Steel Construction.
- Ahmad, S., Hakeem, I. and Maslehuddin, M. (2016), "Development of an optimum mixture of ultra-high performance concrete", *Eur. J. Environ. Civil Eng.*, **20**(9), 1106-1126.
- ASTM A370 (2014), "Standard Test Methods and Definitions for Mechanical Testing of Steel Products", West Conshohocken, PA: ASTM International.
- ASTM C293/C293M (2016), "Standard Test Method for Flexural Strength of Concrete (Using Simple Beam with Center-Point Loading)", West Conshohocken, PA: ASTM International.
- ASTM C39/C39M (2017), "Standard Test Method for Compressive Strength of Cylindrical Concrete Specimens", West Conshohocken, PA: ASTM International.
- ASTM E8/E8M-13 (2013), "Standard Test Methods for Tension Testing of Metallic Materials", West Conshohocken, PA: ASTM International.
- Basu, P.K., Sharif, A.M. and Ahmed, N.U. (1987a), "Partially prestressed composite beams. II", *J. Struct. Eng.*, **113**(9), 1926-1938.
- Basu, P.K., Sharif, A.M. and Ahmed, N.U. (1987b), "Partially prestressed continuous composite beams. I", *J. Struct. Eng.*, **113**(9), 1909-1925.
- Birtel, V. and Mark, P. (2006), "Parameterised Finite Element Modelling of RC Beam Shear Failure", Abaqus User's Conference, 95-108.
- Chen, S., Wang, X. and Jia, Y. (2009), "A comparative study of continuous steel-concrete composite beams prestressed with external tendons: experimental investigation", *J. Constr. Steel Res.*, **65**(7), 1480-1489. <https://doi.org/10.1016/j.jcsr.2009.03.005>.
- Committee, A.C.I., Institute, A.C. and Standardization, I.O. (2008) "Building code requirements for structural concrete (ACI 318-08) and commentary", American Concrete Institute.
- Ding, F.X., Liu, J., Liu, X.M., Guo, F.Q. and Jiang, L.Z. (2016), "Flexural stiffness of steel-concrete composite beam under positive moment", *Steel Compos. Struct.*, **20**(6), 1369-1389. <http://dx.doi.org/10.12989/scs.2016.20.6.1369>.
- Elremaily, A. and Yehia, S. (2006), "Use of External Prestressing to Improve Load Capacity of Continuous Composite Steel Girders", in Structures Congress 2006, Structural Engineering and Public Safety, 1-10.
- Fang, G., Wang, J., Li, S. and Zhang, S. (2016), "Dynamic characteristics analysis of partial-interaction composite continuous beams", *Steel Compos. Struct.*, **21**(1), 195-216. <http://dx.doi.org/10.12989/scs.2016.21.1.195>.
- Kim, S.H., Park, S.J., Heo, W.H. and Jung, C.Y. (2015), "Shear resistance characteristic and ductility of Y-type perfobond rib shear connector", *Steel Compos. Struct.*, **18**(2), 497-517. <http://dx.doi.org/10.12989/scs.2015.18.2.497>.
- Kim, S.H., Jung, C.Y. and Ahn, J.H. (2011), "Ultimate strength of composite structure with different degrees of shear connection", *Steel Compos. Struct.*, **11**(5), 375-390. <http://dx.doi.org/10.12989/scs.2011.11.5.375>.
- Lee, J. and Fenves, G.L. (1998), "Plastic-damage model for cyclic loading of concrete structures", *J. Eng. Mech.*, **124**(8), 892-900. [https://doi.org/10.1061/\(ASCE\)0733-9399\(1998\)124:8\(892\)](https://doi.org/10.1061/(ASCE)0733-9399(1998)124:8(892)).
- Lin, W., Yoda, T., Taniguchi, N., Kasano, H. and He, J. (2013), "Mechanical performance of steel-concrete composite beams subjected to a hogging moment", *J. Struct. Eng.*, **140**(1), 4013031. [https://doi.org/10.1061/\(ASCE\)ST.1943-541X.0000800](https://doi.org/10.1061/(ASCE)ST.1943-541X.0000800).
- Lin, W. and Yoda, T. (2013), "Experimental and numerical study on mechanical behavior of composite girders under hogging moment", *Int. J. Adv. Steel Constr.*, **9**(4), 309-333.
- Liu, J., Ding, F.X., Liu, X.M. and Yu, Z.W. (2016), "Study on flexural capacity of simply supported steel-concrete composite beam", *Steel Compos. Struct.*, **21**(4), 829-847. <https://doi.org/10.12989/scs.2016.21.4.829>.
- Lubliner, J., Oliver, J., Oller, S. and Oñate, E. (1989), "A plastic-damage model for concrete", *Int. J. Solids Struct.*, **25**(3), 299-326. [https://doi.org/10.1016/0020-7683\(89\)90050-4](https://doi.org/10.1016/0020-7683(89)90050-4).
- Nie, J., Tao, M., Cai, C.S. and Li, S. (2011), "Analytical and numerical modeling of prestressed continuous steel-concrete composite beams", *J. Struct. Eng. Am. Soc. Civil Engineers*, **137**(12), 1405-1418. [https://doi.org/10.1061/\(ASCE\)ST.1943-541X.0000409](https://doi.org/10.1061/(ASCE)ST.1943-541X.0000409).
- Rodrigues, J.P.C. and Laím, L. (2014), "Experimental investigation on the structural response of T, T-block and T-Perfobond shear connectors at elevated temperatures", *Eng. Struct.*, **75**, 299-314.
- Samaaneh, M.A., Sharif, A.M., Baluch, M.H. and Azad, A.K. (2016), "Numerical investigation of continuous composite girders strengthened with CFRP", *Steel Compos. Struct.*, **21**(6), 1307-1325. <http://dx.doi.org/10.12989/scs.2016.21.6.1307>.
- Simulia (2013), Getting Started with Abaqus, Keyword Edition.
- Sharif, A.M., Samaaneh, M.A., Azad, A.K. and Baluch, M.H. (2015), "Use of CFRP to maintain composite action for continuous steel-concrete composite girders", *J. Compos. Constr.*, **20**(4), 1-10. [https://doi.org/10.1061/\(ASCE\)CC.1943-5614.0000645](https://doi.org/10.1061/(ASCE)CC.1943-5614.0000645).
- Standardization, E.C. (2004), "Design of composite steel and concrete structures. Part 1-1: General rules and rules for buildings", in Eurocode.
- Thirumalaiselvi, A., Anandavalli, N., Rajasankar, J. and Iyer, N.R. (2016), "Numerical evaluation of deformation capacity of laced steel-concrete composite beams under monotonic loading", *Steel Compos. Struct.*, **20**(1), 167-184. <http://dx.doi.org/10.12989/scs.2016.20.1.167>.
- Vasdravellis, G. and Uy, B. (2014), "Shear strength and moment-shear interaction in steel-concrete composite beams", *J. Struct. Eng.*, **140**(11), 4014084. [https://doi.org/10.1061/\(ASCE\)ST.1943-541X.0001008](https://doi.org/10.1061/(ASCE)ST.1943-541X.0001008).
- Wang, B., Huang, Q. and Liu, X. (2017), "Deterioration in strength of studs based on two-parameter fatigue failure criterion", *Steel Compos. Struct.*, **23**(2), 239-250. <https://doi.org/10.12989/scs.2017.23.2.239>.
- Xiang, T., Yang, C. and Zhao, G. (2015), "Stochastic creep and shrinkage effect of steel-concrete composite beam", *Adv. Struct. Eng.*, **18**(8), 1129-1140. <https://doi.org/10.1260/1369-4332.18.8.1129>.
- Zhan, Y., Ma, Z.J., Zhao, R., Li, G. and Xiang, T. (2016), "Interface behavior between steel and concrete connected by bonding", *J. Bridge Eng.*, **21**(6), 4016026. [https://doi.org/10.1061/\(ASCE\)BE.1943-5592.0000813](https://doi.org/10.1061/(ASCE)BE.1943-5592.0000813).
- Zhou, M., Zhang, J., Zhong, J. and Zhao, Y. (2016), "Shear stress calculation and distribution in variable cross sections of box girders with corrugated steel webs", *J. Struct. Eng.*, **142**(6), 4016022. [https://doi.org/10.1061/\(ASCE\)ST.1943-541X.0001477](https://doi.org/10.1061/(ASCE)ST.1943-541X.0001477).
- Zhou, W., Jiang, L., Huang, Z. and Li, S. (2016), "Flexural natural vibration characteristics of composite beam considering shear deformation and interface slip", *Steel Compos. Struct.*, **20**(5), 1023-1042. <https://doi.org/10.12989/scs.2016.20.5.1023>.